Heat Flux Estimates Across A6 and A7 WOCE Sections

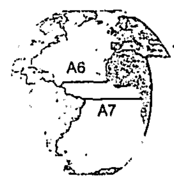

F. Marin, LPO (CNRS-IFREMER-UBO), Brest, France; Y. Gouriou and B. Bourlès, ORSTOM, Brest, France. fmarin@ifremer.fr

One of the main goals of the WOCE programme is to assess meridional heat fluxes across various hydrographic sections in the three oceans. Indeed, except in the North Atlantic Ocean, where numerous convergent estimates exist, the magnitude and sometimes even the sign of oceanic heat fluxes may appear questionable, and the seasonal variability of this heat transport has yet to be documented. Table 1 yields some estimates of meridional heat transports, based on hydrological transects, for the Atlantic Ocean between 30°S and 30°N: heat transport is northward at all latitudes, and seems to increase from 30°S to 11°N, particularly in the tropical region, where the heat gain by the ocean is the strongest.

To study the contribution of the equatorial area in this heat gain by the ocean, the A7 and A6 WOCE sections were carried out aboard N/O l'Atalante as part of the CITHER project: A7 took place in January 1993 along 4.5°S, A6 in February–March 1993 along 7.5°N. Fig. 1 shows the location of the 175 considered hydrographic stations; station spacing is about 70 km in the midocean, but shorter near the coasts to follow the bathymetric features. A RDI 75 kHz ship-mounted ADCP provided absolute velocities from 28 metres to about 700 metres depth. Heat flux estimates are first presented for both A6 and A7 sections. Then, a study of the heat flux variability across the 7.5°N section is presented, based on data collected during the two ETAMBOT (Etude du Transport Atlantique Meridien de Bord Ouest equaTorial) cruises; the latter have repeated the WOCE A6 section west of 35°W, in September 1995 and April 1996.

Method and results

Following Hall and Bryden (1982), the meridional heat flux is split into four components:

$$H = H_{WBC} + H_{Ek} + H_B + H_b$$

H_{WBC} is the contribution of the shallow-western boundary current on the continental shelf, down to 200 metres; H_{Ek} is the wind-generated Ekman transport across the section; H_B is the vertically-averaged barotropic component and H_b the baroclinic geostrophic part:

$$H_b = \rho \cdot C_p \cdot \int \theta'(x) \cdot v'(x) dx$$

where ρ is the density of water, C_p the specific heat at constant pressure, θ the potential temperature, v the geostrophic velocity, and where primes refer to baroclinic quantities, i.e. the difference between in-situ values and their vertical average. This method assumes that there is no volume transport across the whole section, that the vertically-averaged (or barotropic) temperature $\bar{\theta}$ is constant along the section (equal to 4.54°C and 4.23°C respectively for 7.5°N and 4.5°S sections) and that absolute currents are only composed of geostrophic and Ekman currents. Under these conditions, we do not need to determine a reference velocity for geostrophic currents, and the barotropic heat transport becomes:

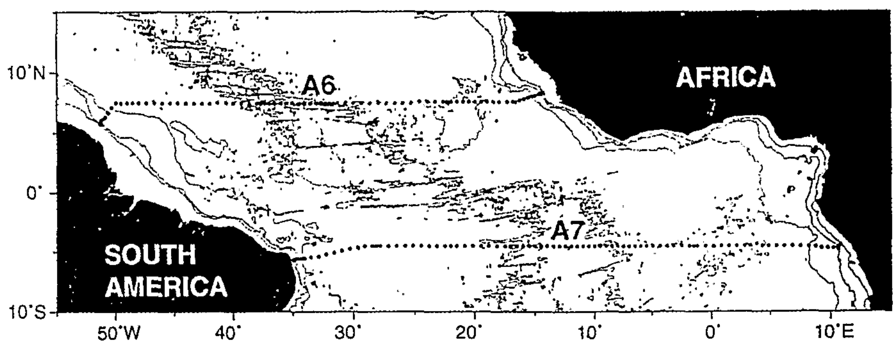

Figure 1. Location of the 175 hydrological stations of interest along 7.5°N and 4.5°S in the Atlantic. Isobaths of 200, 2000 and 4000 metres are shown.

$$H_B = -\rho \cdot C_p \cdot \bar{\theta}\left(\int T_{Ek}(x)dx + T_{WBC}\right)$$

Unlike the 4.5°S section where the 200 m isobath is near the coast, H_{WBC} can not be neglected for the 7.5°N section: there, the continental shelf extends 170 km off French Guiana. No estimate of this transport is available for the period of the cruise. Bourlès et al. (1998) collected various estimates of this transport between 1989 and 1996, and found a mean volume transport of 3.8±1.2 Sv, with no clear seasonal cycle. Such an estimate leads, for a mean temperature of 26.8°C, to a heat transport of 0.42±0.13 PW. These values are retained in this paper.

Two methods for the computation of Ekman heat transports are compared in this note:

- first, the traditional approach based on climatological wind stresses is used; because ship measured winds are not available for the cruise, we have used Servain et al. (1996)'s monthly pseudo-windstresses linearly interpolated at the date and the location of the stations. Wind stresses τ are computed using the bulk formula:

$$\tau = \rho_a \cdot C_D \cdot |u| \cdot u$$

where $\rho_a = 1.25 kg.m^{-3}$ is the air density and $C_D = 1.15\ 10^{-4}$ the drag coefficient. Following the Ekman theory, the mass transport T_{Ek} and the heat transport H_{Ek} will then be expressed as:

ISN : 1029-1725

$$T_{Ek} = \int v_{Ek} \cdot dx; \; H_{Ek} = \rho C_p \int \left(\bar{\theta}_{Ek}(x) \cdot v_{Ek}(x) dx\right);$$
$$v_{Ek}(x) = \tau_y(x) / (\rho \cdot f)$$

where f is the Coriolis parameter, the cross-section component of wind and the Ekman layer temperature that will be replaced in our computation by the sea-surface temperature. The following Ekman volume and heat transports are obtained: 11.5 Sv and 1.23 PW across 7.5°N, -9.3 Sv and -1.01 PW across 4.5°S. The western parts of each section are the major contributors for both estimates. To evaluate the error bars on these estimates, Ekman transports are computed for December, January and February; we get the following average estimates: 11.7±1.0 Sv and 1.28±0.08 PW for 7.5°N, -13.7±3.2 Sv and -1.37±0.20 PW for 4.5°S. Thus, whereas estimates for the northern section prove to be constant for the period of the cruise, Ekman transports across 4.5°S change significantly when considering the average for the three months, because the Ekman transports are particularly weak in January. The problem of knowing whether the two sections may be considered as synoptic is already raised.

- secondly, following Chereskin and Roemmich (1991) and Wijffels et al. (1992), we assume that the Shipborne ADCP (S-ADCP) absolute velocities are only composed of the geostrophic and Ekman currents; ageostrophic components, but the Ekman velocity, are then neglected. The problem is then to choose a reference level where ageostrophic velocities cancel, i.e. where S-ADCP and geostrophic velocities merge. For 7.5°N, this level is chosen at 600 metres, and Fig. 2 presents the profiles of ageostrophic, geostrophic and ADCP transports versus depth; a slab layer extrapolation is applied for S-ADCP currents at the surface. The ageostrophic transport appears to vanish at 65–80 m, for potential density between 24.5 and 25.3, precisely in the core of the thermocline, even though a weaker ageostrophic signal persists deeper; Ekman dynamics is likely to govern this surface-trapped transport of 7.7 Sv and 0.68 PW. If we choose a linear extrapolation at the surface instead of a slab layer, these estimates become 8.7 Sv and 0.77 PW. We will arbitrarily synthetise these results and give the following estimates of Ekman transports across 7.5°N: 8.2±0.5 Sv and 0.72±0.05 PW. The case of the 4.5°S section is more complex: the ageostrophic velocities no longer vanish at the core of the thermocline. The 4.5°S section is indeed at the location of the South Equatorial UnderCurrent (SEUC), with speeds greater than 40 cm/s in its core at a depth of about 180 m: the assumption that ageostrophic velocities other than Ekman ones are negligible is all the more questionable here, as Coriolis terms are of less importance at 4.5°S. Particularly, the thermocline does no longer play the role of a barrier between the strong wind-generated signal above and the weaker ageostrophic one beneath. Consequently, besides the level of cancellation of ageostrophic velocities, the depth of the Ekman layer must be specified arbitrarily; we choose it at the core of the thermocline, as for 7.5°N, and find Ekman transports equal to -4.0±1.7 Sv and -0.53±0.20 PW, with error bars representing the difference between a slab layer and a linear extrapolation at the surface.

The two methods used to compute the Ekman transports give divergent results: S-ADCP deduced wind-generated velocities lead to weaker estimates

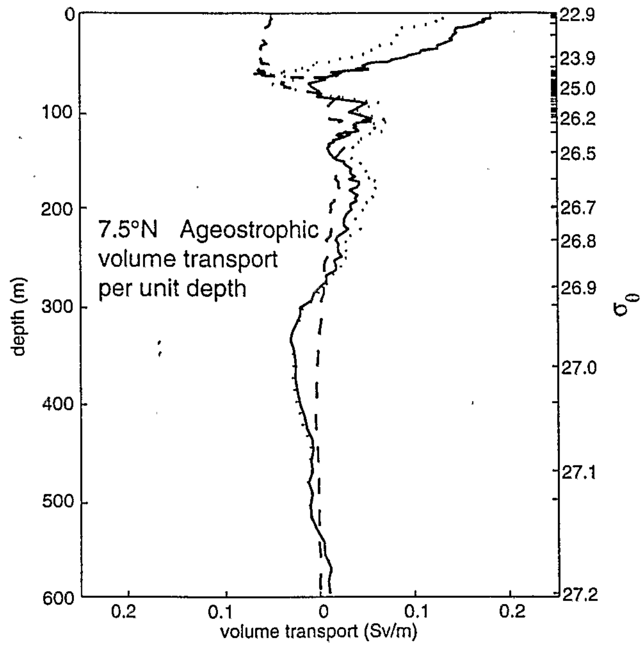

Figure 2. S-ADCP (dotted), geostrophic (dashed) and ageostrophic (solid line) transport per unit depth across 7.5°N (in Sv/m). Geostrophic currents are chosen to merge with S-ADCP currents on average on the depth range 500–600 metres.

Table 1. Estimates of meridional heat fluxes across various transatlantic sections between 30°S and 30°N. Positive values represent northward heat transports. Error bars account for uncertainties on the method of computation and/or on seasonal variabilities.

References	Latitude	Heat Flux (PW)
Molinari et al. (1990)	26.5°N	1.21±0.34
Johns et al. (1997)	26.5°N	1.44±0.33
Hall and Bryden (1982)	25°N	1.2±0.3
Roemmich et al. (1984)	24.5°N	1.2±0.2
Klein et al. (1995)	14.5°N	1.22 (annual) 1.37±0.42 (February)
Friedrichs and Hall (1995)	11°N	1.1 (annual) 0.30±0.18 (May)
Klein et al. (1995)	8°N	1.18 (annual) 1.69±0.52 (May)
Speer et al. (1994)	11°S	0.6±0.17
Holfort (1994)	11°S	0.7±0.25
Holfort (1994)	19°S	0.69±0.25
Holfort (1994)	23°S	0.36±0.25
Holfort (1994)	30°S	0.40±0.25

Table 2. *Volume and heat fluxes across A6 and A7 sections for various Ekman transport computations:*
a - with Servain et al. (1996)'s pseudo-windstresses interpolated at the location and the date of CTD stations.
b - with wind-generated velocities deduced from the comparison of geostrophic and S-ADCP currents.
c - with Servain et al. (1996)'s pseudo-windstresses interpolated at the location of CTD stations, averaged for January-February-March.

Section	H_{WBC}	H_{Ek}	H_b	H_B	H
A6 a (Sv)	3.8±1.2	11.5±0.5	-	-15.3±1.7	-
(PW)	0.42±0.13	1.23±0.05	-0.13	-0.29±0.04	1.23±0.14
A6 b (Sv)	3.8± 1.2	8.2±0.5	-	-12.0±1.7	-
(PW)	0.42±0.13	0.86±0.05	-0.13	-0.21±0.03	0.94±0.16
A6 c (Sv)	3.8±1.2	11.7±1.0	-	-15.5±2.2	-
(PW)	0.42±0.13	1.28±0.08	-0.13	-0.29±0.04	1.28±0.17
A7 a (Sv)	-	-9.3±1.2	-	9.3±1.2	-
(PW)	-	-1.01±0.14	2.13	0.16±0.02	1.28±0.12
A7 b (Sv)	-	-4.0±1.7	-	4.0±1.7	-
(PW)	-	-0.53±0.20	2.13	0.07±0.03	1.67±0.14
A7 c (Sv)	-	-13.7±3.2	-	13.7±3.2	-
(PW)	-	-1.37±0.20	2.13	0.24±0.06	1.00±0.04

for both 7.5°N and 4.5°S. For 7.5°N, the underestimation may be the consequence of the large mesoscale variability in this region (Richardson et al., 1994). The problem seems greater for the 4.5°S section, because, besides the large monthly variability in climatological data, the assumption that ageostrophic velocities, except Ekman ones, are negligible seems no longer valid there.

The baroclinic heat fluxes are easier to estimate, because they are directly computed from hydrological data. These fluxes occur essentially in the upper ocean, where both temperatures and velocities take their greater values. We find the following estimates: -0.13PW for the 7.5°N section, and 2.13 PW across 4.5°S. It must be noted that the estimate for 7.5°N is subject to an important error bar, given the strikingly variable character of this flux near the western boundary of the basin (Fig. 3).

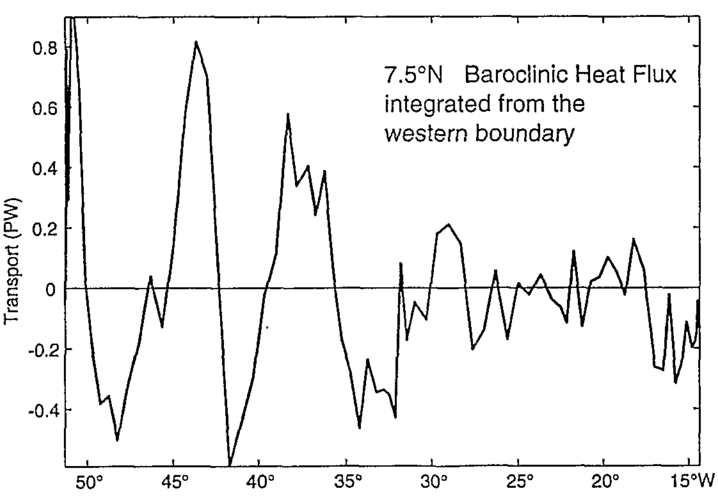

Figure 3. Baroclinic heat flux, integrated from the western boundary, across 7.5°N. The unit is PW.

The last component to evaluate is the barotropic contribution, whose computation is based on the assumption of no volume flux across a zonal transect. For each section, the estimates are computed separately from the two different values obtained for the Ekman volume transport. The results are reported on Table 2. Heat flux estimates are very sensitive to the computation method of Ekman transports: the S-ADCP method gives an amazing heat loss from South to North, which can not be explained with traditional estimates for air-sea fluxes. Results with Servain et al. (1996)'s pseudo-windstresses lead to a net heat gain of approximately 0.3 PW within error bars if we consider the winds averaged on the trimester of the cruise. We prefer to retain these values (1.28±0.17 PW across 7.5°N and 1.00±0.14 PW across 4.5°S) as seasonally significant, even though we have in mind that a huge month-to-month variability exists across the southern transect.

Seasonal variability across 7.5°N

ETAMBOT 1 and 2 cruises repeat the 7.5°N section west of 35°W, in a region that largely contributes to the heat fluxes across 7.5°N; if we complete the 7.5°N section east of 35°W with Levitus (1982) climatological data, we can estimate heat flux variability across 7.5°N and compare them with the numerical model results – Sarmiento (1986), Philander and Pacanowski (1986), Böning and Hermann (1994). The estimates for each component of the heat fluxes are summarised in Table 3; Ekman transports are computed here from Servain et al. (1996)'s climatological pseudo-windstresses, for the month of the campaign. Of particular interest are the important weakening of Ekman transports in April, that causes a sensitive decreasing of total heat flux across the section, and the non-negligible seasonal variability on baroclinic heat fluxes: in September, we must estimate the latter flux halfway between 0.30 PW for July–August–September and -0.41 PW for October–November–December. Fig. 4 reproduces the seasonal variability seen by different models; our estimates, with their error bars, are also represented. Within error bars, the agreement between our direct computations and the results of numerical models is striking: the seasonal cycle is reproduced, but our data do not allow to conclude whether the heat flux across 7.5°N can take negative values or not.

Table 3. Heatflux components across 7.5°N from ETAMBOT campaigns. Sections are completed east of 35°W with Levitus (1994)'s data. Error bars refer to the seasonal variability.

	ETAMBOT 1 (September 1995)		ETAMBOT 2 (April 1996)	
	Western half	Eastern half	Western half	Eastern half
H_{WBC}	0.45		0.42±0.13	
H_{Ek}	0.10±0.07	-0.10±0.07	0.97±0.15	0.28±0.05
H_b	-0.23	-0.05±0.35	0.06	-0.13
H_B	-0.08±0.08		-0.29±0.21	
H	0.09±0.49		1.31±0.29	

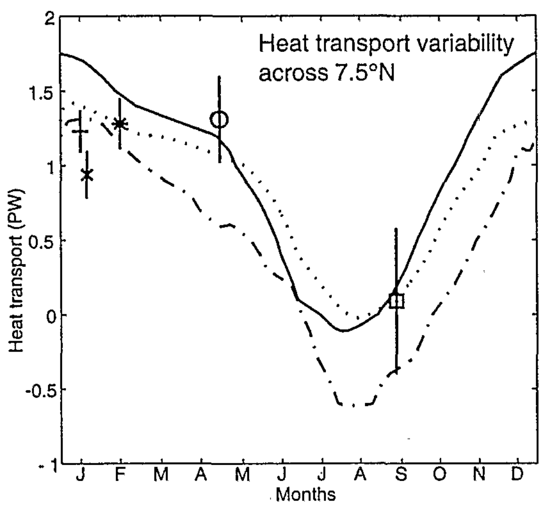

Figure 4. The seasonal variability of the meridional heat flux across 7.5°N, as seen by numerical models [Sarmiento, 1986 (solid line); Philander and Pacanowski, 1986 (dotted-dashed); Böning and Herrmann, 1994 (dotted line)] and our estimates - where vertical bars refer to error bars - from CITHER 1 [windstress for the campaign (cross), ageostrophic method (x) and trimestrially-averaged windstress (star)], ETAMBOT 1 (square) and ETAMBOT 2 (circle) data. The unit is PW.

Acknowledgements

This investigation was supported by the Programme National d'Etude de la Dynamique du Climat (PNEDC) and its WOCE/France subprogramme.

References

Böning, C. W., and P. Hermann, 1994: Annual cycle of poleward heat transport in the ocean: results from High-Resolution modeling of the North Equatorial Atlantic. J. Phys. Oceanogr., 24, 91–107.

Bourlès, B., Y. Gouriou, R. Chuchla, and C. Colin, 1998: On the northward warm water flow over the continental shelf of French Guiana. Submitted to J. Geophys. Res.

Chereskin, T. K., and D. Roemmich, 1991: A comparison of measured and wind-driven Ekman transport at 11°N in the Atlantic Ocean. J. Phys. Oceanogr., 21, 869–878.

Hall, M. M., and H. L. Bryden, 1982: Direct estimate and mechanism of ocean heat transport. Deep-Sea Res., 29, 3A, 339–359.

Holfort, J., 1994: Grossräumige Zirkulation und meridionale Transporte im Südatlantik. Ph.D. thesis, 118 pp., Ber. Inst. Meeresk. Kiel.

Klein, B., R. L. Molinari, T. J. Müller, and G. Siedler, 1995. A transatlantic section at 14.5°N: meridional volume and heat fluxes. J. Marine Res., 53, 929–957.

Levitus, S., 1982: Climatological atlas of the world ocean, NOAA Prof. Paper 13, U.S. Govt. Printing Office, 173 pp.

Philander, S. G. H., and R. C. Pacanowski, 1986. The mass and heat budget in a model of the tropical Atlantic Ocean. J. Geophys. Res., 12, 14212–14220.

Richardson, P. L., G. E. Hufford, R. Limeburner, and W. S. Brown, 1994: N.B.C retroflection eddies. J. Geophys. Res., 99, 5081–5093.

Sarmiento, J. L., 1986. On the North and Tropical Atlantic heat balance. J. Geophys. Res., 11, 677–689.

Servain, J., J. N. Stricherz, and D. M. Legler, 1996: TOGA Pseudo-wind stress Atlas 1985–1994 - volume 1: Tropical Atlantic.

Wijffels, S. E., E. Firing, and H. L. Bryden, 1992: Direct observations of the Ekman balance at 10°N in the Pacific. J. Phys. Oceanogr., 24, 1666–1679.

WOCE/CLIVAR Workshop on Ocean Modelling for Climate Studies,

NCAR, Boulder, CO, USA, 10–13 August 1998

The workshop aims to bring together ocean and climate modellers and observationalists, in order to understand how current and future observational datasets can be used to guide the development of ocean models, particularly those used to study climate. The goals are: (1) to develop an understanding and consensus in the modelling community of how well different aspects of ocean dynamics need to be represented in order to achieve realistic simulations of the ocean's role in climate variability on decadal time scales, and (2) to develop a consensus of benchmark data sets for quantitative model tests that could lead to more co-ordination, transparency and feedback between individual model development efforts.

The group of invited participants is expected to produce a research plan directed towards clarifying the role of certain small-scale ocean processes and their numerical representation in simulations of climate variability.

Scientific Committee: C. Böning (chair), M. England, P. Gent, D. Haidvogel, W. Large, L. Talley, E. Tziperman, D. Webb, J. Willebrand, R. Wood, C. Wunsch.